Research Article

Received: 11 March 2008 Revised: 5 June 2008 Accepted: 21 July 2008 Published online in Wiley Interscience: 9 October 2008

(www.interscience.wiley.com) DOI 10.1002/jctb.2038

Optimization and analysis of nickel adsorption on microwave irradiated rice husk using response surface methodology (RSM)

Magesh Ganesa Pillai,[a] I. Regupathi,[b] M. Helen Kalavathy,[a] T. Murugesan[c,a] and Lima Rose Miranda[a]*

Abstract

BACKGROUND: The removal of heavy metals using adsorption techniques with low cost biosorbents is being extensively investigated. The improved adsorption is essentially due to the pores present in the adsorbent. One way of improving the porosity of the material is by irradiation of the precursor using microwaves. In the present study, the adsorption characteristics of nickel onto microwave-irradiated rice husks were studied and the process variables were optimized through response surface methodology (RSM).

RESULT: The adsorption of nickel onto microwave-irradiated rice husk (MIRH) was found to be better than that of the raw rice husk (RRH). The kinetics of the adsorption of Ni(II) from aqueous solution onto MIRH was found to follow a pseudo-second-order model. Thermodynamic parameters such as standard Gibbs free energy (ΔG°), standard enthalpy (ΔH°), and standard entropy (ΔS°) were also evaluated. The thermodynamics of Ni(II) adsorption onto MIRH indicates that it is spontaneous and endothermic in nature. The response surface methodology (RSM) was employed to optimize the design parameters for the present process.

CONCLUSION: Microwave-irradiated rice husk was found to be a suitable adsorbent for the removal of nickel(II) ions from aqueous solutions. The adsorption capacity of the rice husk was found to be 1.17 mg g^{-1}. The optimized parameters for the current process were found as follows: adsorbent loading 2.8 g (100 mL)$^{-1}$; Initial adsorbate concentration 6 mg L^{-1}; adsorption time 210 min.; and adsorption temperature 35 °C.

Keywords: adsorption; response surface methodology; microwave irradiation; central composite rotary design; nickel

NOTATION

a_f	Multilayer adsorption capacity and intensity of adsorption (mg g^{-1})
a_L	Langmuir constants (L mg^{-1})
b	Langmuir adsorption intensity constant (L mg^{-1})
b_f	Freundlich isotherm exponent
k_c	Equilibrium constant
k,	Number of factors in cube portion of design
q_e,	Equilibrium adsorption capacity (mg g^{-1})
q_t	Amount of Nickel ion adsorbed per unit mass of adsorbent at time (mg g^{-1})
t	Contact time (min)
$x_i x_j$,	Dimensionless coded value of ith variable
A	Adsorbent concentration (g (100 mL)$^{-1}$)
B	Initial adsorbate concentration of Solution (mg L^{-1}),
C	Adsorption time (min)
D	Adsorption temperature (°C)
C_{Ae}	Equilibrium concentration of Ni (II) on the solution (mg L^{-1})
C_{Be}	Equilibrium concentration of Ni (II) on the adsorbent (mg L^{-1})
C_o	Initial concentration of adsorbate in solution (mg L^{-1})
F	Number of points in cube portion of design
K_1	First-order rate constant (min^{-1})
K_2	Second-order rate constant (g mg^{-1} min^{-1})
K_L	Langmuir constants (L g^{-1})
R	Universal gas constant (kJ kg^{-1} mol^{-1} K^{-1})
R^2	Coefficient of determination
T	Temperature (K)
V	Volume of adsorbent (L)
V_o	Initial volume of adsorbent (L)
X	Independent variable
X_i,	The natural value of the ith variable
X_{max}	Highest limits of the ith variable

* *Correspondence to: Lima Rose Miranda, Department of Chemical Engineering, A.C. College of Technology, Anna University, Chennai 600025, India. E-mail: limamiranda2007@gmail.com*

a *Department of Chemical Engineering, A.C. College of Technology, Anna University, Chennai 600025, India*

b *Department of Chemical Engineering, National Institute of Technology Karnataka, Mangalore, India*

c *Chemical Engineering Programme, Universiti Teknologi PETRONAS, Bandar Seri Iskandar, 31750, Tronoh, Perak, Malaysia*

X_{min} Lowest limits of the *i*th variable
Y, Y_i Predicted response
Greek letters
α Variables for the axial points
β_{ii} iith interaction coefficient
β_o ith linear variable coefficient
ΔH° Changes in enthalpy
ΔS° Changes in entropy
ΔG° Changes in free energy

INTRODUCTION

Technological advances and rapid industrialization have led to an increase in the quantity of effluents discharged into water bodies. The effluents contain both organic and inorganic pollutants which are highly toxic and have to be treated to conform to international norms. Nickel, a heavy metal, although an essential constituent for both plants and animals, is required in very low concentrations. Increased discharge of this heavy metal into the environment has to be contained since nickel exposure to humans causes headache, dermatitis, dizziness, dry cough, nausea, vomiting, and cyanosis leading to capillary, hepatic and renal damage, nervous disabilities, chest pain, cancer in lungs, nose, bones, etc. In general it is a listed carcinogenic for all living organisms. During the last few years, new regulations coupled with increased law enforcements concerning wastewater discharges have been established in many countries. Due to the toxicity of the metal, the World Health Organization (WHO) and Euro Environmental Contracts (EEC) have set the international standard for nickel to be discharged into surface waters at 0.02 mg L^{-1}.[1]

A wide variety of conventional and non-conventional technologies have been developed throughout the years for the reduction and removal of most metals including nickel. These techniques include solvent extraction, ion exchange, reverse osmosis, electrodialysis, precipitation, flocculation, sorption, activated carbon adsorption and membrane separation processes[2–4] (basically physical, chemical, physico-chemical and biological in nature). Of all these methods mentioned above for the removal of nickel, reduction, precipitation and coagulation techniques have been accepted industrially. However, they are not efficient and create sludge. Ion-exchange and reverse osmosis, although effective and efficient are expensive. These techniques have disadvantages, such as high capital and operational costs or they require the treatment and disposal of the residual metal sludge. Hence cheaper and more viable alternatives are being considered of which adsorption onto agricultural/biological waste is one.[5,6]

The use of agricultural residues or industrial by-products having biological activity has received considerable attention for the adsorption of metal ions. In recent years, a number of agricultural materials such as moss peat,[7] coconut husk,[8] chitosan,[9] coir pith, rice husk,[10] tea leaves,[11] and almond husk,[12] have been investigated for the removal of toxic metals from aqueous solutions. Most of these materials contain functional groups associated with proteins, polysaccharides, lignin, and cellulose as major constituents. Metal uptake is believed to occur through a sorption process involving these functional groups. Previous investigations of the removal of heavy metal ions have utilized either raw rice husk as a source material or have carbonized it. Activation of any carbonaceous material is carried out with the intention of increasing its surface area. In the present work, microwave irradiation of the raw material was studied as a possible route to enhancing adsorption. Microwave-irradiated rice husk (MIRH) has been utilized as a sorbent for the adsorption of heavy metals using conventional adsorption procedures. Further, to optimize the process variables for the adsorption of nickel, response surface methodology (RSM) was used. RSM aims at developing a mathematical model to describe the effects and relationships of the main process variables, to maximize adsorption.

EXPERIMENTAL PROCEDURE

Methods and materials

Preparation of Adsorbent

The adsorbent rice husk was obtained from a local rice mill and washed thoroughly with distilled water to remove all impurities present. The prepared rice husk was exposed to microwave irradiation for 2 min at a microwave output power of 180 W.

Chemicals

A stock solution of nickel (II) ions (1000 mg L^{-1}) was prepared by dissolving 4.787 g of $NiSO_4.7H_2O$ in 1 L of distilled water. All chemicals (sodium citrate, iodine, dimethylglyoxime, concentrated hydrochloric acid and ammonia buffer solution) used for analysis were of analytical grade and purchased from Ranbaxy Fine Chemicals Ltd, India.

Experimental method

A temperature controlled incubator shaker was used for all adsorption batch experiments with a constant agitation speed of 180 rpm. A UV–Vis spectrophotometer (Hitachi U 2002, Chennai, India) was utilized to analyze the nickel metal concentrations in the treated water. Isotherm studies were carried out in 250 mL Erlenmeyer flasks. Each flask was filled with 100 mL of adsorbate solution which was varied from 5 to 45 mg L^{-1}. The adsorbent loading ranged between 1 and 5 g $(100\ mL)^{-1}$ of sample solution. All experiments were conducted using double distilled water. The samples taken at different time intervals (0 to 300 min) were analyzed using a UV spectrophotometer by forming a complex with dimethylglyoxime ($\lambda_{max} = 470$ nm). The equilibrium adsorption capacity was calculated using:

$$q_e = [(C_o - C_e)V]\frac{1}{M} \quad (1)$$

Experimental design

Central composite rotary design

The object of any process is to achieve a level of design at which the response reaches an optimum. Although many techniques are available to do this, response surface methodology (RSM) is one of the best.[13] The main advantages of this method include an understanding of how the test variables (process variables) affect the selected process response, the determination of any possible interrelationships among the test variables, and the characterization of the combined effect that all test variables may have on the process response. From the literature, it was found that although RSM has been widely used for other processes, no studies had been conducted and reported on microwave-activated rice husk adopting RSM as the optimization tool.

A five level four-factor central composite rotary design (CCRD) was performed using the software Design expert 7.1.1® (Stat-Ease Inc. Minneapolis, USA) to find the interactive effects of the four variables *A* (adsorbent concentration; g $(100\ mL)^{-1}$, *B* (initial adsorbate concentration of solution; mg L^{-1}), *C* (adsorption time;

Table 1. Level of variables considered for the adsorption of nickel using central composite rotary design (CCRD)

S.No	Variable	Name	Variable Level				
			-2 ($-\alpha$)	-1	0	$+1$	2 ($+\alpha$)
1	*A*	Adsorbent Loading (g (100 mL)$^{-1}$)	1	2	3	4	5
2	*B*	Initial Adsorbate Concentration (mg L^{-1})	5	15	25	35	45
3	*C*	Time (min.)	35	100	165	230	295
4	*D*	Temperature (° C)	20	25	30	35	40

min), and *D* (adsorption temperature; °C) on the adsorption of nickel(II) ions.[14] The design of these experiments was intended to reduce the number of experiments with a wide range of predicted response *Y*. In the rotary design, the standard error, which depends on the coordinates of the point on the response surface at which *Y* is evaluated and on the coefficients β, is the same for all points that are at the same distance from the central point. The value of α for rotatability depends on the number of points in the factorial portion of the design, which is given by

$$\alpha = (F)^{1/4} \text{ where } F = (2)^K \tag{2}$$

where *F* is the number of points and *k* the number of factors in the cube portion of the design: *K* being 4, $F = 2^4$ (= 16) points and $\alpha = 2$. The range of the independent variables is based on the conditions screened prior to optimization. The level of variables considered for the CCRD and the array of experiments in terms of coded and actual terms are given in Tables 1 and 2, respectively.

In the experimental design, all variables are coded for statistical calculation according to the following equation

$$x_i = \frac{\alpha[2X_i - (X_{max} - X_{min})]}{[X_{max} - X_{min}]} \tag{3}$$

where x_i is the dimensionless coded value of the *i*th variable, X_i the natural value of the *i*th variable, and X_{max} and X_{min} are the highest and the lowest limits of the *i*th variable, respectively. Once the desired range of variables is defined, they are coded to lie at ± 1 for the factorial points, 0 for the center points and $\pm\alpha$ for the axial points. The matrix consists of a two-level full factorial design, six center points, eight axial points and 16 fact points.[15] Based on this table, experiments were conducted to obtain the response, i.e. the percentage of nickel adsorbed was measured at the values of the independent variables detailed in the experimental design matrix. These experimental data are used to validate the model of the adsorption process. The sequence of experiments was randomized in order to minimize the effects of uncontrolled factors.

Table 2. Independent variables for the adsorption of nickel using central composite rotary design (CCRD)

Run order	Coded				Actual			
	A	*B*	*C*	*D*	*A*	*B*	*C*	*D*
1	0	0	2	0	3	25	295	30
2	0	0	0	2	3	25	165	40
3	0	0	0	0	3	25	165	30
4	1	−1	−1	−1	4	15	100	25
5	0	0	0	0	3	25	165	30
6	0	0	0	0	3	25	165	30
7	0	0	0	−2	3	25	165	20
8	1	−1	1	1	4	15	230	35
9	1	1	1	1	4	35	230	35
10	1	1	1	−1	4	35	230	25
11	1	−1	−1	1	4	15	100	35
12	−1	−1	−1	1	2	15	100	35
13	0	2	0	0	3	45	165	30
14	−1	−1	1	−1	2	15	230	25
15	0	0	0	0	3	25	165	30
16	1	1	−1	−1	4	35	100	25
17	0	−2	0	0	3	5	165	30
18	1	1	−1	1	4	35	100	35
19	−1	−1	1	1	2	15	230	35
20	−2	0	0	0	1	25	165	30
21	−1	1	1	−1	2	35	230	25
22	−1	1	−1	1	2	35	100	35
23	0	0	0	0	3	25	165	30
24	−1	1	−1	−1	2	35	100	25
25	0	0	−2	0	3	25	35	30
26	0	0	0	0	3	25	165	30
27	2	0	0	0	5	25	165	30
28	−1	1	1	1	2	35	230	35
29	1	−1	1	−1	4	15	230	25
30	−1	−1	−1	−1	2	15	100	25

Statistical method

A second-order polynomial equation was considered for all the experimental data, obtained from regression of the response:

$$Y_i = \beta_o + \sum_i \beta_i x_i + \sum_{ii} \beta_{ii} x_i^2 + \sum_{ij} \beta_{ij} x_i x_j \tag{4}$$

where Y_i the predicted response, $x_i x_j$, the independent variables, β_i the ith linear variable coefficient, β_{ij}, the *ij*th interaction coefficient, and independent variables *A*, *B*, *C* and *D*. In this study, a second-order polynomial equation was derived as

$$Y = \beta_o + \beta_1 A + \beta_2 B + \beta_3 C + \beta_4 D + \beta_{11} A^2 + \beta_{22} B^2 + \beta_{33} C^2 + \beta_{44} D^2 + \beta_{12} AB + \beta_{13} AC + \beta_{14} AD + \beta_{23} BC + \beta_{24} BD + \beta_{34} CD \tag{5}$$

Response surface graphs were plotted for all experimental data by regression analysis using the statistical software 'Design expert 7.1.1®. The statistical parameters were examined using analysis of variance (ANOVA). A second-order polynomial was

(a)

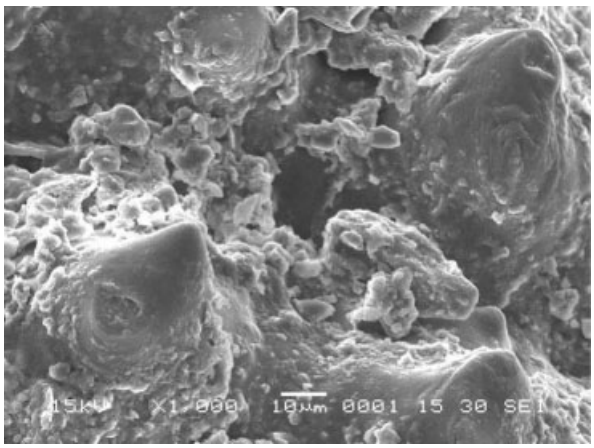

(b)

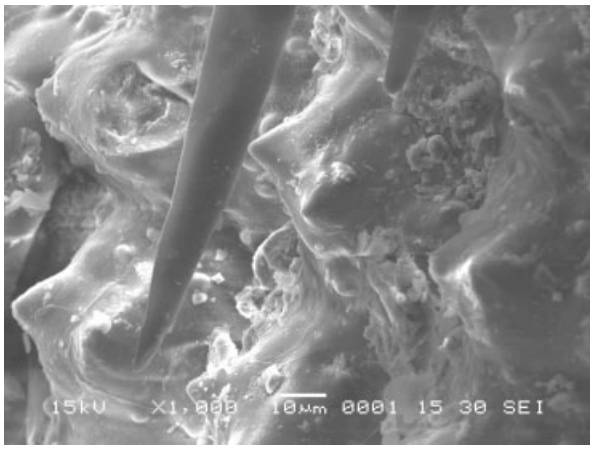

Figure 1. SEM image of (a) raw rice husk (RRH); (b) microwave-irradiated rice husk (MIRH).

employed to fit the experimental data. The implications of the model equations and terms were evaluated by F-test. The quality of fit of the polynomial model equation was expressed by the coefficient of determination (R^2), adjusted R^2 and 'adequate precision'. The fitted polynomial equation was expressed as three-dimensional surface plots to visualize the relationship between the responses and the experimental levels of each factor used in the design. The combination of different optimized parameters, which gave maximum response, i.e. maximum adsorption, was tested experimentally to validate the model.

RESULTS AND DISCUSSION

Microstructure determination

The material when subjected to microwave irradiation loses some of the volatile matter and moisture content. As the drying proceeds, the outer layers of the rice husk become rigid and their final volume is fixed early in the drying. The tissues split and rupture internally, cracks are formed in the inner structure when the interior finally dries, and the internal stresses pull the tissue apart. The dried rice husk then contains numerous holes, forming an open structure.[16,17] A scanning electron microscope (SEM) was employed to investigate the surfaces and the internal structures of rice husk. SEM micrographs (Fig. 1(a), 1(b)) showed that the sample was almost fully dense with large grains in the central part. Thin hairline cracks were observed on the surface of the material. The grain size was smaller in magnitude at the surface than at the centre of the specimen. The large difference in microstructure is due to the extremely high heating rate generated. Microwaves caused violent evaporation of water in cells, followed by a collapse of cell structure and partial disconnection of cells. The interesting point, however, is not the temperature gradient itself, but its direction. The microstructure clearly shows that the heat was mainly generated in the bulk of the sample and transported from the bulk to the environment. This type of temperature gradient can only be generated by microwave heating. Microwave drying is caused by water vapour pressure differences between interior and surface regions, which provide a driving force for moisture transfer. Porosity is strongly affected by the drying method and conditions; an increase in porosity was observed in the dried materials.[18] The microstructure of MIRH showed higher nickel ion adsorption rates than raw rice husk under different operating conditions. Figure 2(a), 2(b) and 2(c) show a comparison between MIRH and RRH. It is clearly observed in all plots and under all operating conditions that MIRH shows better adsorption capability than RRH. Microwave irradiation is a process by which, the inherent moisture content of any material can be reduced, the movement of the water molecules is from the centre of the material to the outer surface, and this creates an increased porous microstructure in the irradiated material. The enhanced porosity is the key factor improving the adsorption capacity of the rice husk.

Effect of initial metal ions concentration and adsorbent dosage on adsorption capacity

Figure 3 shows the effect of initial concentration on the adsorption capacity of nickel at various initial nickel concentrations for a temperature of 30 °C and adsorbent loading of 3 g (100 mL)$^{-1}$. The removal of Ni(II) increases with time and attains saturation in about 150 min, the degree of removal of adsorbate was initially rapid (up to 50 min) gradually decreasing with time until it reached equilibrium (150 min). From Fig. 3 it is observed that the amount of Ni(II) ion adsorbed increased with increasing in initial concentration of metal ions. The percentage removal of nickel became almost insignificant after 150 min due to rapid exhaustion of the adsorption sites. The resistance to the uptake of metal from solution decreases with increasing metal ion concentration. The rate of adsorption also increased with increasing initial concentration due to the enhanced driving force.[19,20] After the adsorbed material forms a monolayer (ion), the capacity of the adsorbent is exhausted and then the uptake rate is controlled by the rate at which the adsorbate is transported from the exterior to the interior sites of the adsorbent particles. The data indicates that the initial metal concentration determines the equilibrium concentration, and also determines the uptake rate of metal ions and the kinetic character.

Figure 4 shows the effect of initial adsorbent dosage on the adsorption capacity, indicating that the uptake of nickel per gram of adsorbent decreases with increasing adsorbent dosage. Although there is an increase in the total number of sites, there is no significant increase in the active sites per gram, thereby causing a decrease in the adsorbate uptake.[21] Thus, the driving force for mass transfer between the bulk liquid phase and the solid phase decreases with the passage of time.[22]

Effect of temperature on adsorption capacity

The adsorption of nickel(II) ion onto MIRH at different temperatures showed an increase in the adsorption capacity when

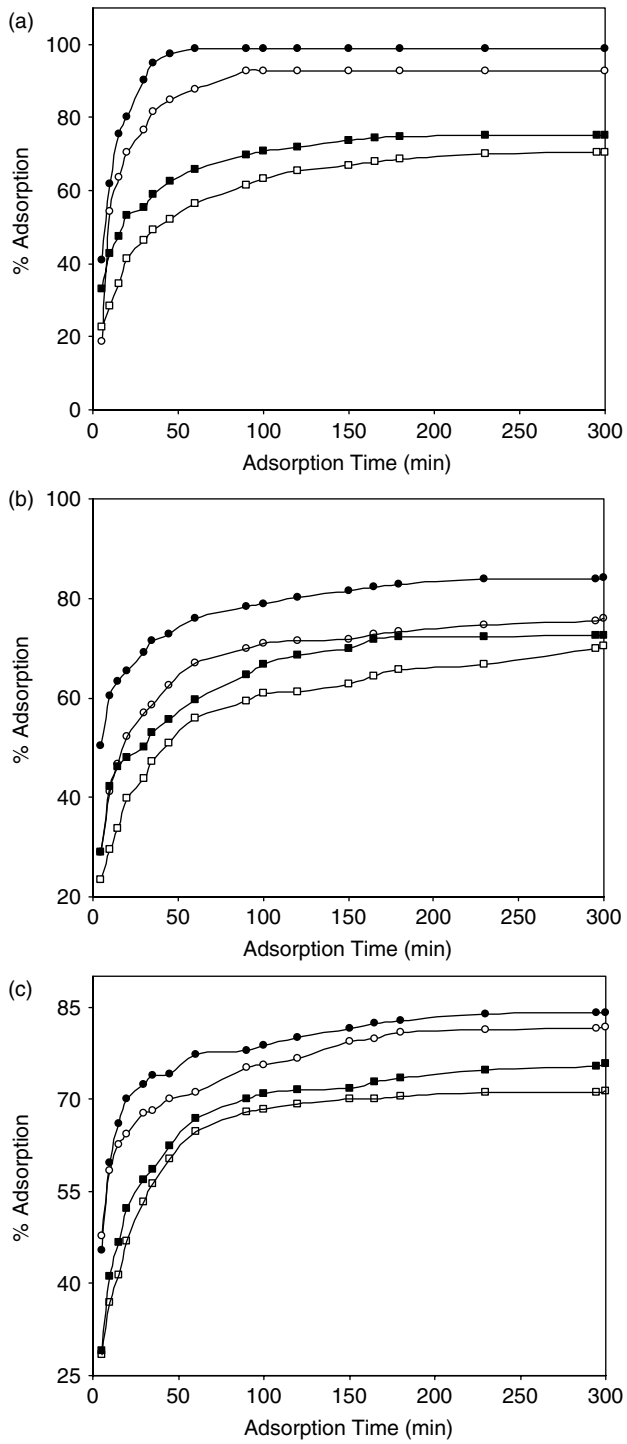

Figure 2. Comparison of percentage adsorption of nickel(II) for raw rice husk (RRH) and microwave irradiated rice husk (MIRH) (a) at different initial adsorbate concentrations (adsorption temperature = 30 °C, adsorbent loading = 3 g(100 mL)$^{-1}$ ● MIRH 5 mg L^{-1}, ○ RRH 5 mg L^{-1}, ■ MIRH 45 mg L^{-1}, □ RRH 45 mg L^{-1}); (b) at different adsorbent loadings (adsorption temperature = 30 °C, initial adsorbate concentration = 25 mg L^{-1} ● MIRH 3 g (100 mL)$^{-1}$, ○ RRH 3 g (100 mL)$^{-1}$, ■ MIRH 1 g (100 mL)$^{-1}$, □ RRH 1 g (100 mL)$^{-1}$, (c) at different adsorption temperatures (initial adsorbent loading = 3 g (100 mL)$^{-1}$, initial adsorbate concentration = 25 mg L^{-1}, ● MIRH 30 °C, ○ RRH 30 °C, ■ MIRH 20 °C, □ RRH 20 °C).

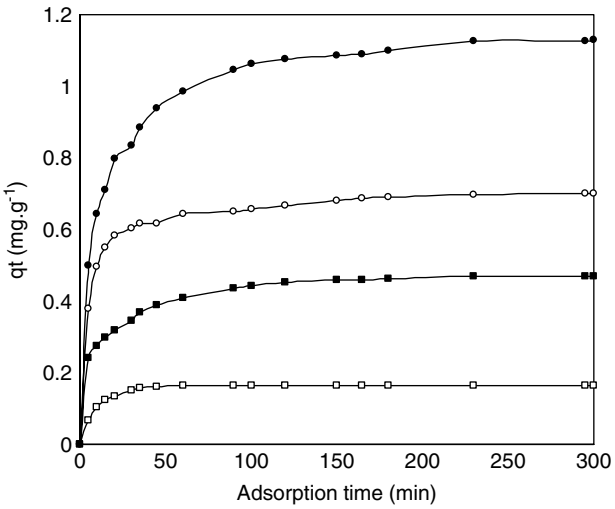

Figure 3. Effect of initial adsorbate concentration on adsorption capacity for nickel (II). (Adsorption temperature = 30 °C, initial adsorbent loading = 3 g (100 mL)$^{-1}$, ● 45 mg L^{-1}, ○ 25 mg L^{-1}, ■ 15 mg L^{-1}, □ 5 mg L^{-1}).

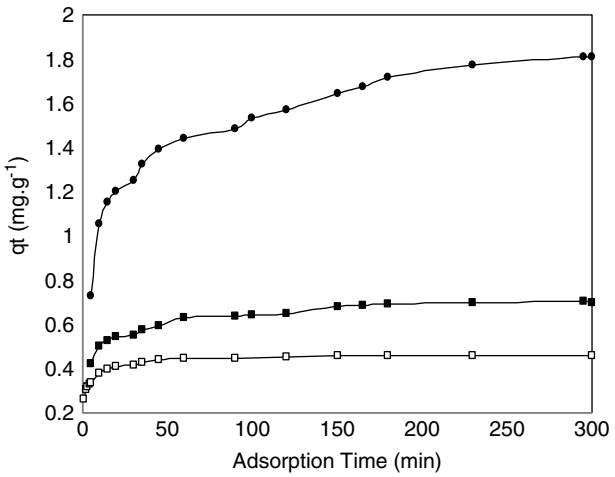

Figure 4. Effect of initial adsorbent dosage on adsorption capacity for nickel (II). (Adsorption temperature = 30 °C, initial adsorbate concentration = 25 mg L^{-1} ● 1 g (100 mL)$^{-1}$, ■ 3 g (100 mL)$^{-1}$, □ 5 g (100 mL)$^{-1}$).

the temperature was increased (Fig. 5). This indicates that the adsorption is endothermic as well as chemical in nature. The increase in temperature increases the mobility of the metal cation; also, swelling within the internal structure of the rice husk enables the metal cation to penetrate further. This effect may also be due to the fact that at higher temperatures an increase in active sites occurs due to bond rupture.[23] The enhancement in the adsorption capacity may be due to the chemical interaction between the adsorbate and the adsorbent, creation of new adsorption sites or the increased rate of intra-particle diffusion of Ni(II) ions into the pores of the adsorbent at higher temperatures.[24] The standard Gibbs free energy was evaluated using

$$\Delta G^{\circ} = -RT.\ln K_c \tag{6}$$

The equilibrium constant K_c was evaluated at each temperature using the relationship

$$K_c = \left[\frac{C_{Be}}{C_{Ae}}\right] \tag{7}$$

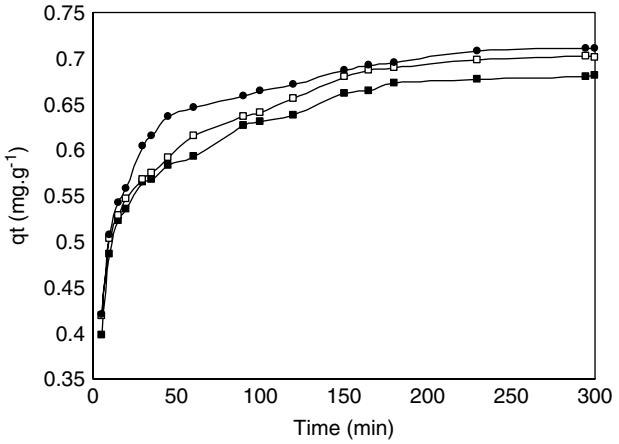

Figure 5. Effect of temperature on adsorption capacity for nickel (II). (Initial adsorbent loading = 3 g (100 mL)$^{-1}$, initial adsorbate concentration = 25 mg L^{-1} ■ 20 °C, □ 30 °C, ● 35 °C).

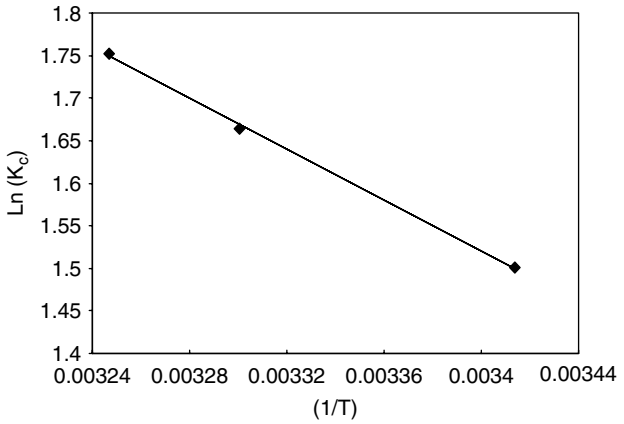

Figure 6. Van't Hoff plot for the adsorption of Ni(II). (Initial adsorbent concentration = 3 g (100 mL)$^{-1}$, Initial adsorbate concentration = 25 mg L^{-1}).

where C_{Be} and C_{Ae} are the equilibrium concentration of Ni(II) on the adsorbent and in the solution, respectively. Standard enthalpy (ΔH°) and entropy (ΔS°) were determined from the van't Hoff equation:

$$\ln K_c = \left[\frac{\Delta S^\circ}{R} - \frac{\Delta H^\circ}{RT}\right] \quad (8)$$

where ΔH° and ΔS° were obtained from the slope and intercept of the van't Hoff plot of ln K_c versus $1/T$, as shown in Fig. 6 and listed in Table 3. The positive value of ΔH° confirms the endothermicity of the adsorption process. The negative values of ΔG° reflect the feasibility of the process and the values become more negative with increasing temperature. Standard entropy determines the disorderliness of adsorption at the solid–liquid interface.[25]

Adsorption isotherm

The dynamic adsorptive separation of solute from solution onto an adsorbent depends upon a good description of the equilibrium separation between the two phases. Many models have been proposed to explain adsorption equilibria, but the most important factor is to have applicability over the entire range of process conditions. The most widely used isotherm models for solid–liquid adsorption are the Langmuir and Freundlich isotherms.

Table 3. Thermodynamic parameters for the adsorption of Ni (II) onto microwave- irradiated rice husk at initial adsorbate concentration of 25 mg L^{-1}, adsorbent loading 3 mg (100 mL)$^{-1}$

T (K)	ΔG° (kJ mol^{-1})	ΔH° (kJ mol^{-1})	ΔS° (J mol^{-1} K^{-1})
293	−3.66		
303	−4.19	12.50	55.12
308	−4.49		

Table 4. Langmuir and Freundlich parameters for the adsorption of Ni(II) onto microwave-irradiated rice husk at constant temperature (30 °C) and adsorbent loading (3 g (100 mL)$^{-1}$)

	Langmuir constants			Freundlich constants		
Temperature	q_{max} (mg g^{-1})	a_L (L mg^{-1})	R^2	a_f (mg g^{-1})	b_f	R^2
303 K	1.17	0.713	0.952	0.4542	0.3579	0.9947

The Langmuir isotherm is based on monolayer adsorption (constant enthalpy of adsorption for all sites) on the active sites of the adsorbent. The data for the uptake of Ni(II) ion have been processed in accordance with the Langmuir isotherm equation:[26]

$$q_e = \left[\frac{K_L C_e}{1 + a_L C_e}\right] \quad (9)$$

The linear form of the Langmuir isotherm is given by

$$\frac{C_e}{q_e} = \left[\left(\frac{1}{K_L} + \frac{a_L C_e}{K_L}\right)\right] \quad (10)$$

where K_L (L g^{-1}) and a_L (L mg^{-1}) are the Langmuir constants. The theoretical maximum monolayer adsorption capacity q_{max} (mg g^{-1}) is given by K_L/a_L.

The Freundlich isotherm gives the relationship between equilibrium liquid and solid phase capacity based on multilayer adsorption (heterogeneous surface). This isotherm is derived from the assumption that the adsorption sites are distributed exponentially with respect to the heat of adsorption[27] and is given by

$$q_e = [a_f C_e^{bf}] \quad (11)$$

with linearized form

$$\log\ q_e = \lfloor(\log\ a_f + b_f\ \log\ C_e)\rfloor \quad (12)$$

where a_f (mg g^{-1}) and b_f are the multilayer adsorption capacity and intensity of adsorption.

The experimental and predicted adsorption capacity using the Langmuir and Freundlich isotherms becomes constant at different adsorbate concentrations (constant temperature 30 °C and adsorbent loading 3g (100 mL)$^{-1}$), along with the regression coefficients, and are listed in Table 4. The Freundlich adsorption isotherm, basically empirical in nature and commonly used to explain metal adsorption data, is also used to describe the nickel uptake. Linear Freundlich adsorption plots were obtained by plotting log (q_e) versus log (C_e) (Fig. 7). The empirical constants a_f and b_f were 0.4542 mg g^{-1} and 0.3579 respectively. These results further proved that MIRH had a higher adsorption capacity at higher initial concentrations.

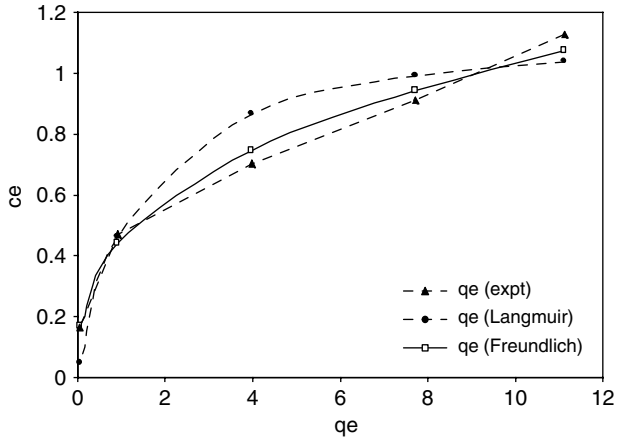

Figure 7. Adsorption isotherms, experimental and predicted by Langmuir and Freundlich models. (Adsorption temperature = 30 °C, initial adsorbent loading = 3 g (100 mL)$^{-1}$).

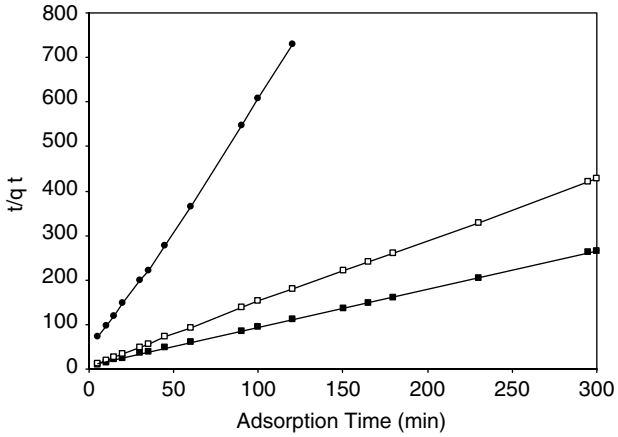

Figure 8. Pseudo-second-order kinetics for Ni(II) adsorption (initial adsorbent dosage 3 g (100 mL)$^{-1}$, adsorption temperature = 30 °C, ● 5 mg L^{-1}, □ 25 mg L^{-1}, ■ 45 mg L^{-1}).

Kinetic studies

The kinetics of the adsorption of Ni(II) were carried out at 30 °C. The data were fitted to Lagergren's pseudo-first-order and pseudo-second-order equations. Lagergren's pseudo-first-order equation[28] is given by

$$\log(q_e - q_t) = \log(q_e) - K_1 t \quad (13)$$

where q_e is the amount of Ni(II) ion adsorbed per unit mass of adsorbent at equilibrium in mg g^{-1}, q_t, is the amount of Ni(II) ion adsorbed per unit mass of adsorbent at any time in mg g^{-1}, and K_1 is the first-order rate constant in min^{-1}. The linearized form of the pseudo-second-order equation[29] is given as

$$\frac{t}{q_t} = \left[\frac{1}{K_2 q_e^2} + \frac{t}{q_e}\right] \quad (14)$$

where K_2 is the second-order rate constant (g mg^{-1} min^{-1}). The experimental and calculated values of the adsorption capacity are given in Table 5. Based on the regression coefficient and the calculated values of adsorption capacity, the adsorption process was found to follow the pseudo-second-order kinetic model (Fig. 8).

Mechanism of mass transfer

The two regions in the q_t versus $t^{0.5}$ suggest that the sorption process proceeds by surface adsorption and intraparticle diffusion (Fig. 9). The initial curved portion of the plot indicates a boundary layer effect, while the second linear portion is due to intraparticle or pore diffusion. The slope of the second linear portion of the plot

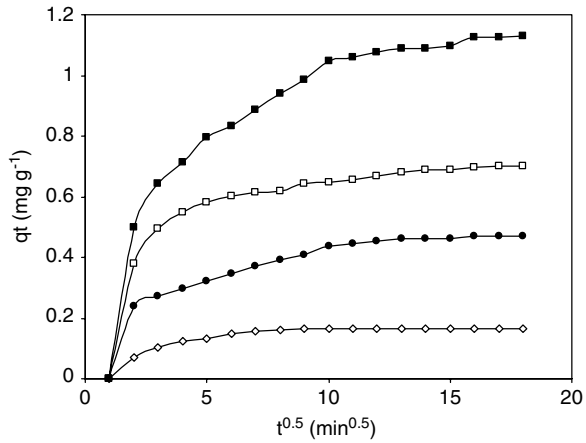

Figure 9. Intraparticle diffusion plot for the adsorption of nickel (II) ion by microwave irradiated rice husk. (○ 5 mg L^{-1}, ■ 15 mg L^{-1}, ● 25 mg L^{-1}, □ 45 mg L^{-1}).

has been defined to yield the intraparticle diffusion parameter k_{id} (mg g^{-1} min$^{-0.5}$). On the other hand, the intercept of the plot reflects the boundary layer effect. The larger the value of the intercept, the larger the contribution of the surface sorption in the rate controlling step. The calculated intraparticle diffusion coefficient k_{id} values are listed in Table 6.

Development of regression model equation

A central composite rotatory design (CCRD) was used to develop a correlation between the adsorption process variables and the percentage adsorption of nickel. CCRD is an extremely powerful

Table 5. Comparison of the pseudo-first-order and pseudo-second-order adsorption rate constants for different initial concentrations

	Pseudo-first-order kinetics			Pseudo-second-order kinetics			
C_o (mg L^{-1})	q_e (cal) (mg g^{-1})	K_1 (min^{-1})	R^2	K_2 ($\times 10^{-4}$ g mg^{-1} min^{-1})	q_e (cal) (mg g^{-1})	R^2	q_e (expt.) (mg g^{-1})
5	0.1698	0.040	0.981	1.03	0.1746	0.998	0.1646
25	0.212	0.0072	0.951	0.2485	0.7122	0.999	0.7007
45	0.517	0.007	0.957	0.0876	1.16	0.999	1.13

Table 6. Intraparticle diffusion rate parameter at different initial concentrations

S. No	C_o (mg L^{-1})	$K_{id} \times 10^3$ (mg g^{-1} $min^{-0.5}$)
1	5	1.28
2	15	1.97
3	25	3.66
4	45	8.69

Table 7. Standard deviation and R^2 for the quadratic model equation

Std. Dev.	0.0784	R-squared	0.9742
Mean	0.7384	Adj R-squared	0.9502
C.V. %	10.62	Pred R-squared	0.8517
PRESS	0.5313	Adeq Precision	26.72

statistical method, since interactions between factors as well as quadratic effects (curvature) are taken into account and quantified in addition to the examination of each factor at five different levels. According to the sequential model sum of squares, the models were selected based on the highest order polynomials for which the additional terms were significant and the models were not aliased. For percentage adsorption of Ni(II) ions, the quadratic model was suggested by the software, which was selected in this case due to the higher order polynomial. The design matrix in actual terms and the experimental results of nickel adsorption by MIRH by CCRD with six center points, eight axial points and 16 fact points are given in Table 2. The application of the RSM based on the estimates of the parameters indicated an empirical relationship between the response and input variables expressed by the following quadratic model:

$$\begin{aligned}\text{adsorption capacity } (Y) &= 0.9983 - 0.6517A + 0.0367B + 0.0012\,C \\ &\quad + 0.0058\,D - 0.0054\,AB - 2.3 \times 10^{-4}\,AC \\ &\quad - 1.17 \times 10^{-3}\,AD + 2 \times 10^{-5}\,BC + 3.15 \\ &\quad \times 10^{-4}\,BD + 1.66 \times 10^{-5}\,CD + 0.1001A^2 \\ &\quad - 1.7 \times 10^{-4}B^2 - 3.6 \times 10^{-6}C^2 - 1.4 \\ &\quad \times 10^{-4}\,D^2 \end{aligned} \quad (15)$$

A positive sign in front of the terms indicates a synergistic effect, whereas a negative sign indicates an antagonistic effect. The quality of the model developed was evaluated based on the correlation coefficient value. The various R^2 values for Equation (15) are given in Table 7. A relatively high R^2 value (close to unity) indicates that there was good agreement between the experimental and model-predicted values (Table 8; Fig. 10). The smaller the standard deviation (Table 7), the better the model, as it gives predicted values closer to the actual value of the response. This indicates that the predicted value for Y is more accurate and closer to the actual value.

The adequacy of the models was further justified through analysis of variance (ANOVA). The ANOVA for the quadratic model for adsorption capacity is listed in Table 9. From the table, the Model '*F*-value' of 40.55 implies that the model was significant and also the values of 'Prob > *F*' less than 0.5 indicates that the model terms were significant. In this case, the process

Table 8. Measured and predicted response for the adsorption of nickel onto MIRH using central composite rotary design (CCRD)

	Factors				Response (*Y*)	
Run order	*A*	*B*	*C*	*D*	Predicted	Actual
1	3	25	295	30	0.6751	0.7017
2	3	25	165	40	0.7170	0.7292
3	3	25	165	30	0.6868	0.6868
4	4	15	100	25	0.3074	0.3162
5	3	25	165	30	0.6868	0.6868
6	3	25	165	30	0.6868	0.6866
7	3	25	165	20	0.6281	0.6609
8	4	15	230	35	0.3018	0.3378
9	4	35	230	35	0.7442	0.7657
10	4	35	230	25	0.6692	0.6994
11	4	15	100	35	0.2978	0.3279
12	2	15	100	35	0.6905	0.6377
13	3	45	165	30	1.1129	1.1183
14	2	15	230	25	0.7179	0.6508
15	3	25	165	30	0.6868	0.6868
16	4	35	100	25	0.6347	0.6773
17	3	5	165	30	0.1251	0.1646
18	4	35	100	35	0.6882	0.7327
19	2	15	230	35	0.7533	0.6883
20	1	25	165	30	1.6067	1.796
21	2	35	230	25	1.3153	1.2628
22	2	35	100	35	1.2989	1.2466
23	3	25	165	30	0.6868	0.6868
24	2	35	100	25	1.2220	1.1634
25	3	25	35	30	0.5778	0.5961
26	3	25	165	30	0.6868	0.6869
27	5	25	165	30	0.5679	0.4235
28	2	35	230	35	1.4137	1.3823
29	4	15	230	25	0.2898	0.3197
30	2	15	100	25	0.6766	0.6327

variables adsorbent loading (*A*), initial adsorbate concentration of solution (*B*), adsorption time (*C*), adsorption temperature (*D*), and the interaction term *AB*, A^2 are the more significant model terms, *AC, BC, BD*, B^2, C^2 have moderate significance, and the interaction terms *AD, CD*, D^2 were insignificant to the response.

Interaction effects of adsorption variables

The adsorption capacity of MIRH at different values of the variables was plotted as three- dimensional response surface contour plots (Fig. 11(a)–(d)), which corresponds to a myriad number of combinations of the two selected variables, while the other two factors remain at their zero level. The plots indicate the mutual interaction of all components with respect to their variables. Based on '*F*' values (Table 9), all the variables were found to be highly significant for the adsorption capacity, whereas the interaction effects of temperature with other variables such as adsorbent loading (*A*) and adsorption time (*C*) had little effect on adsorption capacity. Figure 11(a) shows the combined effect of initial adsorbate concentration and adsorbent loading on adsorption capacity of nickel at constant time (165 min) and temperature (30°C). It is observed that an increase in the initial adsorbate concentration and a decrease

Table 9. Analysis of variance (ANOVA) for response surface quadratic model for adsorption capacity

Source	Sum of squares	Degrees of freedom	Mean square	F Value	*P*-value Prob > F
Model	3.4912	14	0.2494	40.5529	<0.1
A	1.6187	1	1.6187	263.2309	<0.1
B	1.4634	1	1.4635	237.987	<0.1
C	0.0142	1	0.0142	2.3069	0.1496
D	0.0118	1	0.0118	1.9271	0.1854
AB	0.0475	1	0.0475	7.7300	0.0140
AC	0.0034	1	0.0034	0.5627	0.4648
AD	0.00055	1	0.0005	0.0892	0.7693
BC	0.0027	1	0.0027	0.4401	0.5171
BD	0.0039	1	0.0039	0.6459	0.4341
CD	0.0004	1	0.0005	0.0753	0.7875
A^2	0.2749	1	0.2749	44.714	<0.1
B^2	0.0079	1	0.0079	1.2816	0.2754
C^2	0.0062	1	0.0062	1.0155	0.3296
D^2	0.0003	1	0.0003	0.0562	0.8157
Residual	0.0922	15	0.0062		
Lack of Fit	0.0922	10	0.0092	954215.4	<0.1
Pure Error	4.83×10^{-8}	5	9.67×10^{-9}		

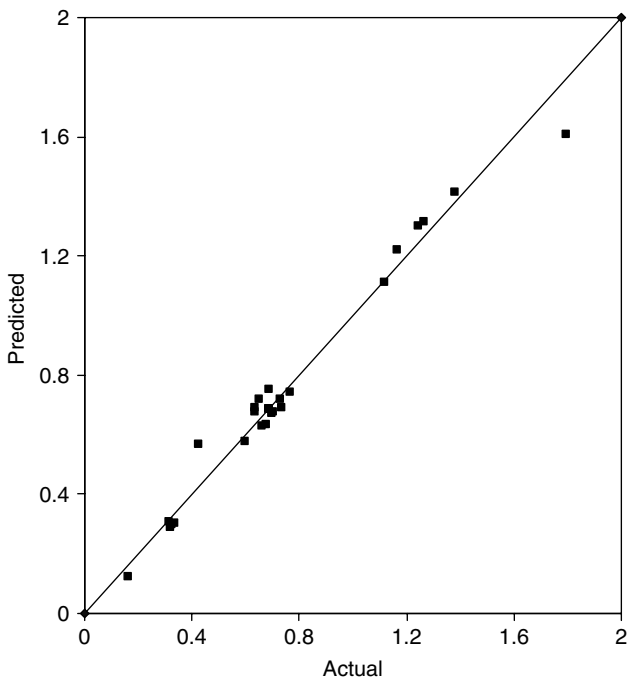

Figure 10. Comparison plot between the experimental and model-predicted adsorption capacity of Ni(II) onto microwave-irradiated rice husk.

in adsorbent loading increased the adsorption capacity of MIRH, which is reflected in the polynomial equation (Equation (15)) in the term *AB*. The adsorption capacity increased for decreasing adsorbent loading and increasing adsorption time, which is evident from Fig. 11(b), for adsorbent loading, adsorption time and adsorption capacity of MIRH at fixed temperature (30°C) and initial adsorbate concentration (25 mg L^{-1}). It was also found that the rate of nickel adsorption increased with time. Figure 11(c) illustrates clearly the interaction between initial adsorbate concentration (*B*) and adsorption temperature (*D*), with adsorbent loading (*A*) fixed at 3g (100 mL)$^{-1}$ of sample and adsorption time (*C*) maintained at 165 min. The adsorption capacity increased with increasing temperature, showing that the adsorption process is endothermic in nature. Figure 11(d) shows the combined effect of adsorption time and temperature on adsorption capacity. The system has an increasing trend for both variables, with adsorbent loading and initial adsorbate concentration maintained at 3 g (100 mL)$^{-1}$ and 25 mg L^{-1}, respectively.

Optimization of adsorption variables

Optimization was carried out after observing all the interaction effects between the adsorption variables. The proficiency of 'point optimization' was used for all the variables. A set of solutions were generated by the Design-Expert 7.1.1 software, to determine the optimum conditions of the process. The optimization study was performed by considering the range of variables used in the experiment (i.e. adsorbent loading 1–5 g (100 mL)$^{-1}$; initial adsorbate concentration 5–45 mg L^{-1}; adsorption time 35–295 min; temperature 20–40 °C) for the maximum response (adsorption capacity, mg g^{-1}) with the desirability value of 1. Initially, the optimization was started at any random value of the individual variables by fixing the target of maximum adsorption capacity and obtaining the optimum values of the variables for the adsorption process, i.e. adsorbent loading 1.5 g (100 mL)$^{-1}$; initial adsorbate concentration 45 mg L^{-1}; adsorption time 280 min and temperature 30 °C with the desirability of 1 for the maximum adsorption capacity of 1.96 mg g^{-1}. The experiment was conducted at the optimized conditions, i.e. where the adsorption capacity of the adsorbent was a maximum and a comparison between the experimental values and model-predicted results was found to be good (Table 10). Thus, the optimum values of the process variables were found to be adsorbent loading (*A*) 1.5 g (100 mL)$^{-1}$; initial adsorbate concentration of solution (*B*) 45 mg L^{-1}; adsorption time (*C*) 280 min.; and the adsorption temperature (*D*) 30 °C.

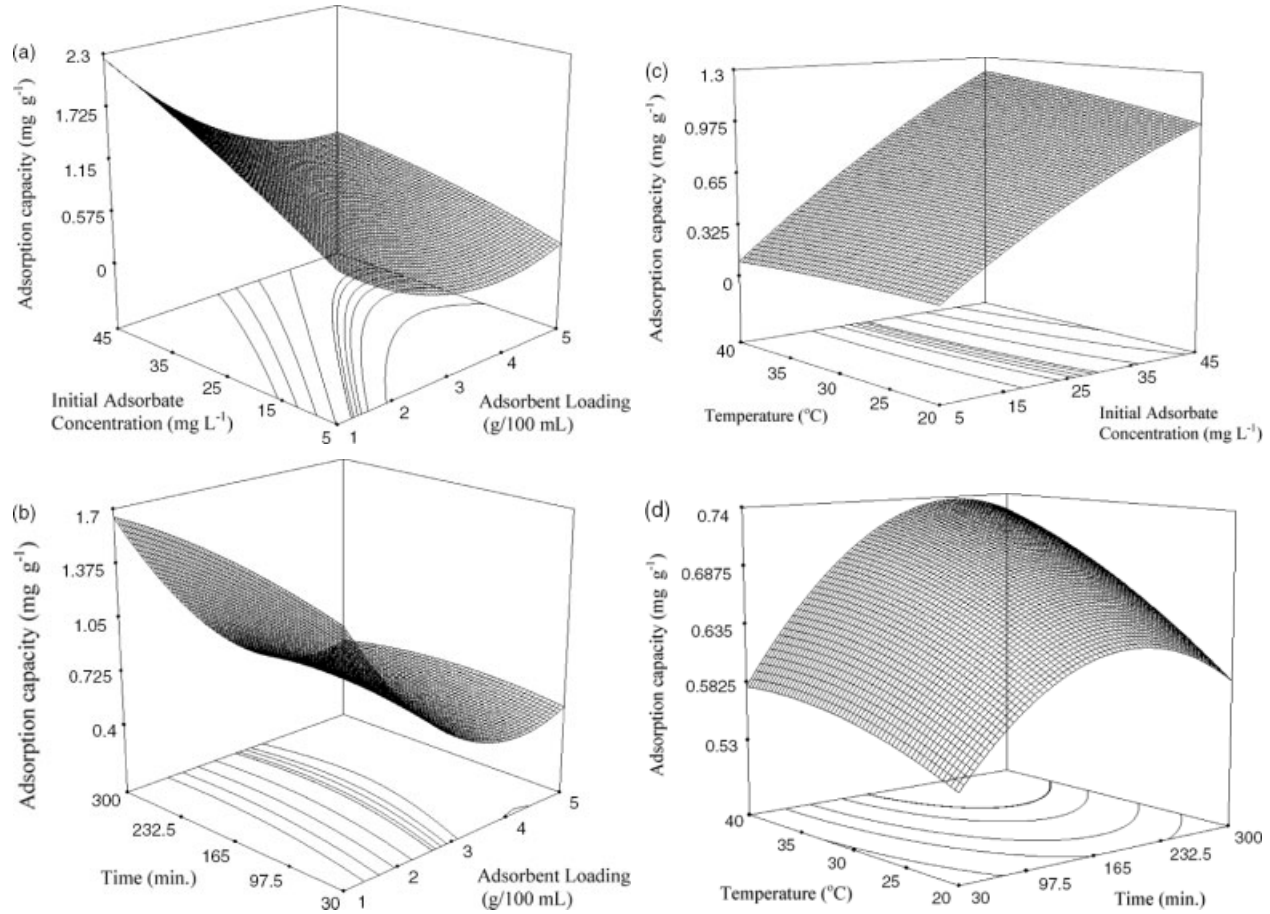

Figure 11. 3D Response surface. (a) Interactive effects of varied initial adsorbent loading and initial adsorbate concentration at adsorption time 165 min and adsorption temperature 30 °C. (b) Interactive effects of varied initial adsorbent loading and adsorption time at initial adsorbate concentration 25 mg L^{-1} and adsorption temperature 30 °C. (c) Interactive effects of initial adsorbate concentration and adsorption temperature at initial adsorbent loading 3g (100 mL)$^{-1}$ and adsorption time 165 min. (d)Interactive effects of adsorption time and adsorption temperature at initial adsorbent loading 3 g (100 mL)$^{-1}$ and initial adsorbate concentration 25 mg L^{-1}.

Table 10. Optimized process variable values for adsorption process

Adsorbent concentration (g (100 mL)$^{-1}$)	Initial adsorbate concentration (mg L^{-1})	Adsorption time (min)	Temperature (° C)	Adsorption capacity (mg g^{-1})	
				Predicted	Experimental
1.5	45	280	30	1.9564	1.9427

CONCLUSIONS

Kinetic and isotherm studies revealed that MIRH, an inexpensive material, could be used as a potential adsorbent for the removal of Ni(II) ions from aqueous solutions. Although the adsorption data fitted the Freundlich isotherm model reasonably well, the maximum adsorption capacity obtained using the Langmuir model compared well with both the experimental data and the q_e values obtained from the pseudo-second-order kinetic model. The kinetics of Ni(II) adsorption were found to follow the pseudo-second-order model. The RSM was used for the optimization and analysis of the adsorption process variables. The existence of interactions between the variables considered for the response was observed to be most significant for *AB, AC, BD*, moderately significant for *CD* and not significant for *AD* and *BC*. The optimum conditions of variables for Ni(II) uptake were adsorbent loading (*A*) 1.5 g (100 mL)$^{-1}$; initial adsorbate concentration of solution (*B*) 45 mg L^{-1}; adsorption time (*C*) 280 min.; and adsorption temperature (*D*) 30 °C.

ACKNOWLEDGEMENTS

The authors wish to acknowledge the grant from the Defense Research and Development Organization (DRDO), Government of India for this research work.

REFERENCES

1 Drinking Water Standards – In the Krewski *et al* Report "*Managing Health Risks from Drinking Water: A Background Paper for the Walkerton Inquiry*". Prepared on behalf of the Ontario Water Works Association and the Ontario Municipal Water Association (2001).

2 Canet L, Ilpide M and Seta P, Efficient facilitated transport of lead, cadmium, zinc and silver across a flat sheet-supported liquid membrane mediated by lasalocid A. *Sep Sci Technol* **37**:1851–1860 (2002).
3 Yan G and Viraraghavan T, Heavy metal removal in a biosorption column by immobilized M. Rouxii biomass. *Bioresources Technol* **78**:243–249 (2001).
4 Zulkali MD, Ahmad AL and Norulakmal NH, Oryza sativa L. husk as heavy metal adsorbent: optimization with lead as model solution. *Bioresource Technol* **97**:21–25 (2006).
5 Shukla MA, Zhang Y, Dubey P, Margrave JL and Shukla SS, The role of sawdust in the removal of unwanted materials from water. *J Hazard Mater* **95**:137–152 (2002).
6 Gerente C, Du Mensil PC, Andres Y, Thibault JF and Cloiree PL, Removal of metal ions from aqueous solution on low cost natural polysaccharides sorption mechanism approach. *React Funct Polym* **46**:135–144 (2000).
7 Lee CK and Low KS, Removal of copper from solution using moss. *Environ Technol* **10**:395 (1989).
8 Tan WT, Ooi ST and Lee CK, Removal of chromium(VI) from solution by coconut husk and palm pressed fibres. *Environ Technol* **14**:277 (1993).
9 Saucedo I, Guibal E, Roulph CH and Cloirec P, Sorption of uranyl ions by a modified chitosan: kinetic and equilibrium studies. *Environ Technol* **13**:1101 (1992).
10 Munaf E, Zein R, Kurniadi R and Kurniadi I, The use of rice husk for removal of toxic metals from waste water. *Environ Technol* **18**:359 (1997).
11 Tee TW and Khan ARM, Removal of lead, cadmium and zinc by waste tea leaves. *Environ Technol* **9**:1223 (1988).
12 Hasar H, Cuci Y and Anadolu , Removal of Cr(VI), Cd(II), and Cu(II) by using activated carbon prepared from almond husk. *J Sci Technol* **21**:1337–1342 (2000).
13 Myers RH and Montgomery DC, *Response Surface Methodology: Process and Product Optimization Using Designed Experiments*. John Wiley (1995).
14 Barros Neto B, Scarminio IS and Bruns RE, *Como Fazer Experimentos*, 2nd edn. Unicamp (2003).
15 Karacan F, Ozden U and Karacan S, Optimization of manufacturing conditions for activated carbon from Turkish lignite by chemical activation using response surface methodology. *Appl Therm Eng* **27**:1212–1218 (2007).
16 Van Arsdel WB, Copley MJ and Morgan AI Jr, *Drying Methods and Phenomena. Food Dehydration*. AVI Pub. Company, Inc. (1973).
17 Wang N and Brennan JG, Changes in structure, density and porosity of potato during dehydration. *J Food Eng* **24**:61–76 (1995).
18 Krokida MK and Maroulis ZB, Quality changes during drying of food materials, in *Drying Technology in Agriculture and Food Sciences,* ed. by Mujumdar AS, Oxford IBH, Delhi, India (2001).
19 Srivatsava VC, Mall ID and Mishra IM, Adsorption of toxic metal ions onto activated carbon, study of sorption behaviour through characterizaion and kinetics. *Chem Eng Process* **47**:1275–1286 (2008).
20 Mall ID, Srivastava VC, Agarwal NK and Mishra IM, Removal of Congo Red from study and equilibrium isotherm analyses. *Chemosphere* **61**:492–501 (2005).
21 Das DD, Mahapatra R, Pradhan J, Das SN and Thakur RS, Removal of Cr(VI) from aqueous solution using activated cow dung carbon. *J Colloid Interface Sci* **232**:235–240 (2000).
22 Pradhan S, Shukla SS and Dorris KL, Removal of nickel from aqueous solutions using crab shells. *J Hazard Mater* **B125**:201–208 (2005).
23 Aksu Z, Determination of the equilibrium, kinetic and thermodynamic parameters of the batch biosorption of nickel(II) ions onto chlorella vulgaris. *Process Biochem* **38**:89–99 (2002).
24 Namasivayam C and Yamuna RT, Adsorption of chromium (VI) by a low-cost adsorbent: biogas residual slurry. *Chemosphere* **30**:561–578 (1995).
25 Karthikeyan T, Rajgopal S and Miranda LR, Chromium (VI) adsorption from aqueous solution by Hevea Brasilinesis sawdust activated carbon. *J Hazard Mater* **B124**:192–199 (2005).
26 Langmuir I, The adsorption of gases on plane surfaces of glass, mica and platinum. *J Am Chem Soc* **40**:361 (1918).
27 Freundlich HZ, die. adsorption. in. losungen (Z). *Phys Chem* **57**:387–470 (1985).
28 Reddad Z, Gerente C, Andres Y and Cloirec P, Adsorption of several metal ions onto a low-cost biosorbent: kinetic and equilibrium studies. *Environ Sci Technol* **36**:2067–2073 (2002).
29 Ho YS and McKay G, Kinetic models for the sorption of dye from aqueous solution by wood. *Trans I Chem E* **76B**:183–191 (1998).

